RSC Advances

ROYAL SOCIETY OF CHEMISTRY

www.rsc.org/advances

Polyelectrolyte Stabilized Bi-Metallic Au/Ag Nanoclusters Modified Electrodes for Nitric Oxide Detection

Perumal Viswanathan, Shanmugam Manivannan and Ramasamy Ramaraj*

School of Chemistry, Centre for Photoelectrochemistry,
Madurai Kamaraj University, Madurai - 625 021, INDIA.
*ramarajr@yahoo.com

Abstract:

In-situ synthesis of bi-metallic Au/Ag nanoclusters (NCs) embedded in poly(acrylamide-co-diallyldimethylammoniumchloride) (PADA) matrix and its application towards the detection of nitric oxide (NO) in nanomolar concentration range were reported. The cationic PADA matrix was used as stabilizer and support material for the preparation of bi-metallic Au/Ag NCs. The electrocatalytic oxidation and electrochemical sensing of NO were studied using the bi-metallic Au/Ag NCs modified electrodes. The modified electrode exhibited synergistic electrocatalytic activity, sensitivity and selectivity towards NO detection when compared to the mono-metallic Au and Ag nanostructures (NCs) modified electrodes. The present bi-metallic Au/Ag NCs modified electrode showed a sensitivity of 3.77 nA/nM, a lowest experimental detection limit of 10 nM with S/N = ~4.9, a fast response time (1 s) and a wide linear range of 10 nM to 0.9 µM towards the detection of NO. Selective sensing of NO was studied in the presence of NO_3^-, CO_2, NH_3 and other common physiological interferences.

Keywords: Gold, silver, gold-silver bi-metal, nanoclusters, polyelectrolyte, modified electrode, NO sensor.

Graphical Abstract:

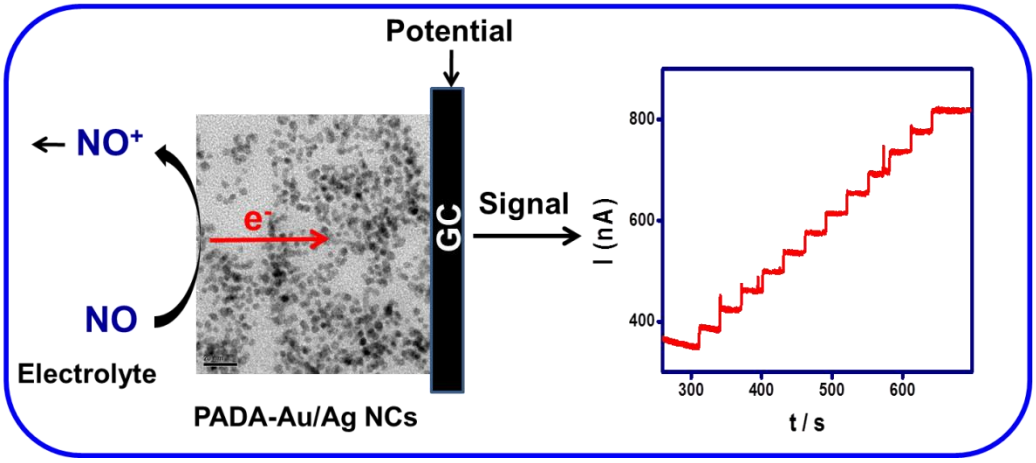

Highlights:

- Cluster-like bi-metallic Au/Ag nanomaterials was prepared.
- Synergistic electrooxidation of NO was observed at Au/Ag NCs modified electrode.
- Electrochemical sensing response time was found to be 1 s.
- Selective sensing of NO in the presence of physiological interferences reported.

1. Introduction

Nitric oxide (NO), an endogenous free radical produced by a collection of enzymes known as nitric oxide syntheses (NOS), is a physiological mediator of the cardiovascular, immune and nervous systems.[1] In brain, NO is produced by neuronal NOS functions as a neurotransmitter and is involved in memory formation.[2] On the other hand, the overproduction of NO is related to neurotoxicity in the brain tissue, such as tissue injury, cellular apoptosis, and ischemia.[3] Furthermore, gas-phase NO levels in exhaled oral and nasal breath may be diagnostically useful for detecting asthma[4] and sinus infections[5], respectively. In cancer biology, NO acts as a tumor progressor or suppressor, which depends on its concentration and lifetime.[6] Due to the short half-life time and low concentration, it is not easy to detect NO in biological samples. Moreover, NO produced by biological means reacts rapidly with oxygen and superoxides present in the bio fluids, which makes the detection of NO even more difficult. The location and concentration of NO governs its biological activity and hence establishing a valid analytical method for measuring NO in physiological pH is important due to its physiological significance. Among the several techniques available for NO sensing such as Griess assay, chemiluminescence, electron spin and paramagnetic resonance spectroscopy, UV–vis spectroscopy, fluorescence and electrochemical methods[7], electrochemical techniques have more advantage over other techniques due to the small electrode size, real-time and direct analysis with high sensitivity.[8] An ideal electrochemical sensor should be cheap, selective and highly sensitive towards the detection of NO. Efforts have been made to improve the sensor performance by way of decreasing the over potential of NO oxidation.

In this connection, nanoscale materials have received significant attention as electrochemical sensors.[9,10] Bi-metallic nanoparticles (NPs) comprising two mono-metallic

counterparts in a single particle exhibit interesting electronic, optical and catalytic properties due to the bi-functional or synergistic effect induced by charge transfer from one metal to the other.[11,12] Among the different bi-metals, Au and Ag have gained increasing interest due to their unique optical and electronic properties.[13] In particular, cluster-like structures are interesting because the properties of nanomaterials are influenced by their inter-particles distance and aggregation state and thus the collective properties are different from the properties of a single nanoparticle.

Our group has previously explored the possible analytical applications of bimetallic Au/Ag nanostructures embedded in polymer matrices.[12,14,15] Herein, we report the preparation of bi-metallic Au/Ag NCs embedded in PADA polymer matrix and the development of a modified electrode for selective and sensitive detection of NO. The mono-metallic Au and Pt NPs have been used as an electrochemical sensor material for NO detection.[9] To the best of our knowledge, this is the first report on NO sensing using bimetallic Au/Ag NCs modified electrode. The bi-metallic Au/Ag NCs were synthesized in aqueous solution at room temperature without using seeds or surfactants. The present electrochemical sensor showed synergistic activity and selectivity towards the detection of NO with fast response time.

2. Experimental section

2. 1 Materials and methods

Chloroauric acid ($HAuCl_4$), silver nitrate ($AgNO_3$), poly(acrylamide-co-diallyldimethylammonium chloride) (PADA), uric acid and D-glucose were received from Sigma-Aldrich. Pure CO_2 gas saturated 0.1 M $KHCO_3$ solution was used as CO_2 source. All other chemicals are analytical grade and were received from Merck. All glassware was thoroughly cleaned with aqua regia (1:3 HNO_3/HCl v/v) (caution: A*qua regia is a powerful oxidizing agent and it should be handled with extreme care.*) and rinsed extensively with

distilled water before use. UV–Visible absorption spectra were recorded using Agilent Technologies 8453 spectrophotometer with a 1 cm quartz cell. High resolution transmission electron microscopy (HRTEM), and selected area electron diffraction (SAED) analyses were conducted in a JEOL JEM 2100 instrument operated at 200 kV. The specimen for the HRTEM analysis was prepared by dropping the colloidal solution onto carbon coated copper grid and dried at room temperature. Energy dispersive X-ray (EDX) analysis was carried out using JEOL Model JSM-6390LV. FT-IR spectra were recorded using Thermo Scientific Nicolet 6700 FT-IR Spectrometer. Electrochemical characterization of mono- and bi-metallic Au/Ag NCs were performed by using a CH Instruments electrochemical workstation (Model–760D).

2. 2 Synthesis of mono-metallic Au and Ag NPs

50 µL of 0.1 M aqueous solution of $HAuCl_4$ or $AgNO_3$ was added to 4.95 mL of 1% PADA solution under vigorous stirring. Then, 200 µL of 0.05 M freshly prepared ice-cold $NaBH_4$ was added slowly to the above solution. The color of the solution immediately turned in to wine red for Au NPs and dark yellow for Ag NPs. The solution was further stirred for 3 h. A homogenous solution was obtained after 3h without any aggregation which confirmed the successful formation of PADA–Au and PADA–Ag NPs.

2. 3 One-step synthesis of bi-metallic Au/Ag NCs

PADA–$Au_{50}Ag_{50}$ NCs was prepared by using the following procedure. In a typical experiment, each 25 µL of 0.1 M solutions of $HAuCl_4$ and $AgNO_3$ was added to 4.95 mL of 1% PADA solution under vigorous stirring. Then, 200 µL of 0.05 M freshly prepared ice-cold $NaBH_4$ was slowly added to the above solution. The color of the solution immediately turned brown and the solution was further stirred for 3 h. The PADA–$Au_{25}Ag_{75}$ and PADA–

$Au_{75}Ag_{25}$ NCs were prepared using corresponding molar ratios of 0.1 M solutions of $HAuCl_4$ and $AgNO_3$ by following the same procedure. The subscripts shown in the $Au_{25}Ag_{75}$, $Au_{50}Ag_{50}$ and $Au_{75}Ag_{25}$ NCs refer to the percentage molar composition of the corresponding metal precursors.

2. 4. Electrochemistry

All the electrochemical experiments were conducted in a single compartment three electrode cell using a CHI760D Electrochemical Workstation, CH Instruments, USA. A GC electrode (3 mm dia) and a platinum wire were used as working and counter electrodes, respectively. Calomel electrode was used as reference electrode. A 5 µL of prepared NCs solution was drop casted onto the cleaned GC surface and allowed to dry for 2 h at room temperature. The modified electrode was soaked in double distilled water for 5 min for swelling and used for electrochemical experiments. 0.1 M phosphate buffer solution (PBS) (pH 7.2) was used as electrolyte for electrocatalysis and sensor studies. Nitrogen gas was bubbled into the cell solution for 25 min prior to each experiment unless otherwise stated.

2. 5 Preparation of NO saturated PBS

All glassware and PBS solution were bubbled with nitrogen gas prior to NO preparation. The NO saturated PBS was prepared using the reported proced ure.[16] Briefly, 2 M of H_2SO_4 was added drop-wise to a saturated $NaNO_2$ solution leading to the production of NO gas through disproportionation reaction of NO_2^- ions in acidic solution. The produced NO gas was bubbled through a 5% (w/v) pyrogallol solution saturated with potassium hydroxide and then 10% (w/v) potassium hydroxide in order to remove other forms of nitrogen oxides. Finally, NO gas was bubbled in PBS and stored in nitrogen-protected environment. The NO standard solutions were prepared by making successive dilutions of the NO saturated PBS. Freshly prepared NO standard solutions were used for all experiments,

and the solutions were kept in a tightly closed glass flask and light-free septum with wrapped black foils. The concentration of saturated NO solution at 20 °C was reported as 1.8 mM.[16]

3. Results and discussion

3. 1 Absorption spectral studies

The formation of mono-metallic Au, Ag NPs and bi-metallic Au/Ag NCs was primarily confirmed by recording their absorption spectra. Fig. 1 shows the absorption spectra obtained for mono- and bi-metallic Au/Ag NCs embedded in PADA matrix. The surface plasmon resonance (SPR) bands of mono- and bi-metallic Au/Ag NCs are strongly dependent on their size, shape, composition of Au or Ag NPs and their local environment.[17–20] Mono-metallic Ag and Au NPs embedded in PADA matrix showed their characteristic SPR absorption maximum (λ_{max}) at 406 (Fig. 1(a)) and 521 nm (Fig. 1(e)), respectively. Bi-metallic Au/Ag NCs prepared using different molar ratios of Au and Ag precursors showed their typical SPR absorption bands in between the mono-metal NCs absorption. The $Au_{75}Ag_{25}$ (Fig. 1(d)) and $Au_{50}Ag_{50}$ NCs (Fig. 1(c)) embedded in PADA matrix showed absorption bands at 515 and 496 nm, respectively. The $Au_{25}Ag_{75}$ NCs embedded in PADA matrix showed a broad absorption band at 417 nm (Fig. 1(b)). The SPR band of the bimetallic Au/Ag NCs was blue-shifted with increasing the concentration of Ag (shift is not linear) (Fig. S1) and this observation suggest that the Au/Ag NCs may be an alloy[21] or hybrid nanostructures. The absorption bands of mono- and bi-metal NCs were plotted against the gold mole fraction (x_{Au}) (Inset Fig. in Fig. S1). The observed broadness and blue shift in the SPR band of Au_{25}/Ag_{75} NCs is attributed to the surface to surface interparticle plasmon coupling of NCs. The interparticle distance in Au_{25}/Ag_{75} NCs is very low than that of other two bi-metal ratios, which is evidenced from the HRTEM images (Fig. 2E).[15,22] The electromagnetic field enhancement may be very large when two resonant particles are brought close to each other and most of the energy is located between the particles. As the

surface electron density depends on the shape or arrangement of the metal atoms in nanoparticle, the electric field on the particle surface varies and this causes variations in the oscillation frequency of the electrons. This indicates that the dimensionality plays a crucial role in determining the position and shape of the SPR band. The observation of SPR band and the noticeable color change of the solutions suggest that the formed bi-metallic Au/Ag NCs are neither a core-shell nor a physical mixture of the mono-metallic Au and Ag NPs. It is evident from literature that two distinguishable SPR bands were observed for physical mixture of mono-metallic Ag and Au NPs.[21] As the absorption spectrum of PADA did not show any absorption band in the wavelength range of 300–1100 nm, the spectral bands obtained for the NCs are essentially due to SPR of Au and Ag NPs.

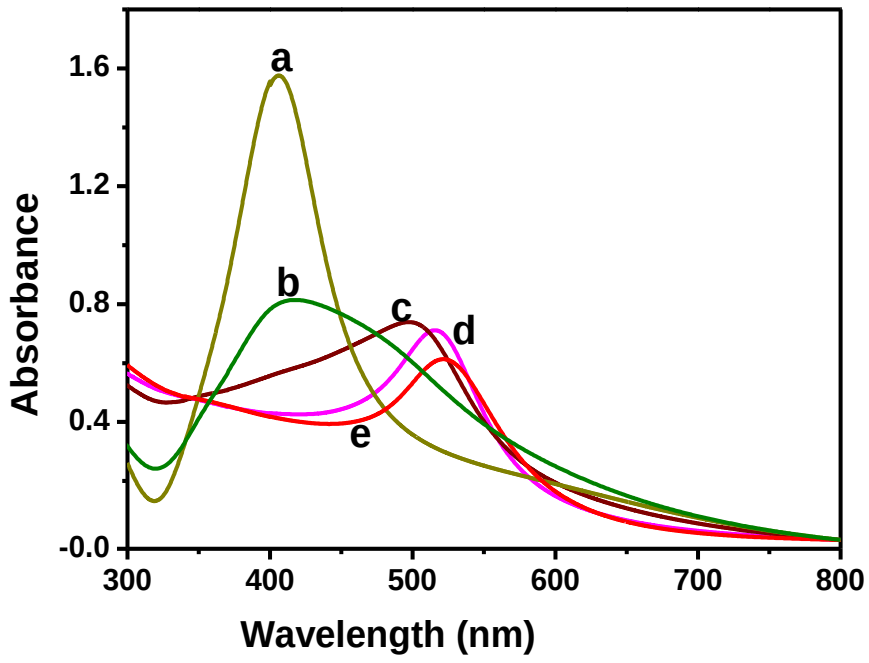

Fig. 1 Absorption spectra obtained for PADA–Ag NPs (a), PADA–$Au_{25}Ag_{75}$ NCs (b), PADA–$Au_{50}Ag_{50}$ NCs (c), PADA–$Au_{75}Ag_{25}$ NCs (d) and PADA–Au NPs (e) solutions.

3. 2 HRTEM and FT-IR studies

The morphology of the PADA stabilized mono-metallic Au, Ag NPs and bi-metallic Au/Ag NCs were studied by HRTEM analysis. It was observed that the well dispersed spherical Ag NPs (Fig. 2(A)) and Au NPs (Fig. 2(C)) with average particle sizes of 13.5 and 7 nm, respectively were formed in the presence PADA matrix. Both Ag and Au NPs showed their characteristic SAED patterns and the *d* spacing values obtained from the SAED patterns correspond to (1 1 1), (2 0 0), (2 2 0) and (3 1 1) crystal planes of Ag (Fig. 2(B)) and (1 1 1), (2 0 0) and (2 2 0) crystal planes of Au (Fig. 2(D)). When compared to the HRTEM images of the mono-metallic Ag and Au NPs, the bi-metallic Au/Ag NCs are smaller in size and have relatively narrow size distribution. The HRTEM images of PADA–$Au_{25}Ag_{75}$ NCs (Fig. 2(E)) reveals that closely associated spherical NCs are formed in the presence of PADA matrix with average particle size of 4.3 nm. The *d* spacing values obtained from the SAED pattern of PADA–$Au_{25}Ag_{75}$ NCs (Fig. 2(F)) correspond to (1 1 1), (2 0 0), (2 2 0) and (3 1 1) crystal planes of Ag and Au. This observation suggests that the $Au_{25}Ag_{75}$ NCs were enriched with both Ag and Au contents. Furthermore, the presence of Au and Ag in the bi-metallic PADA–$Au_{25}Ag_{75}$ NCs were confirmed by EDX spectrum (Fig. S(2)). The atomic percentage obtained from the EDX analysis was merely equal to that of the experimentally calculated atomic percentage of PADA-$Au_{25}Ag_{75}$ NCs. The HRTEM images recorded for PADA–$Au_{50}Ag_{50}$ (Fig. 2(G)) and PADA-$Au_{75}Ag_{25}$ (Fig. 2(H)) NCs also show the spherical shape particles with average particle size of 5.3 and 3.7 nm, respectively. From the HRTEM analysis of mono- and bi-metallic Au/Ag NCs embedded in PADA matrix, it is confirmed that bi-metallic NCs have smaller size and relatively narrow size distribution than the mono-metallic NPs. The Au/Ag NCs embedded in PADA matrix was further confirmed from the FT-IR spectra (Fig. S(3)). The bands observed for PADA at 1665 and 3180 cm^{-1} are due to the stretching vibrations of C=O and N-H bonds, respectively and the bands at 1607 and 1458 cm^{-1} are due to the bending vibration of N-H and C-H bonds[23,24], respectively. In comparison to the

PADA, mono- and bi-metallic Au/Ag nanostructures showed the same FT-IR spectra observed for PADA, which confirms that the prepared mono- and bi-metallic nanostructures are embedded in PADA matrix.

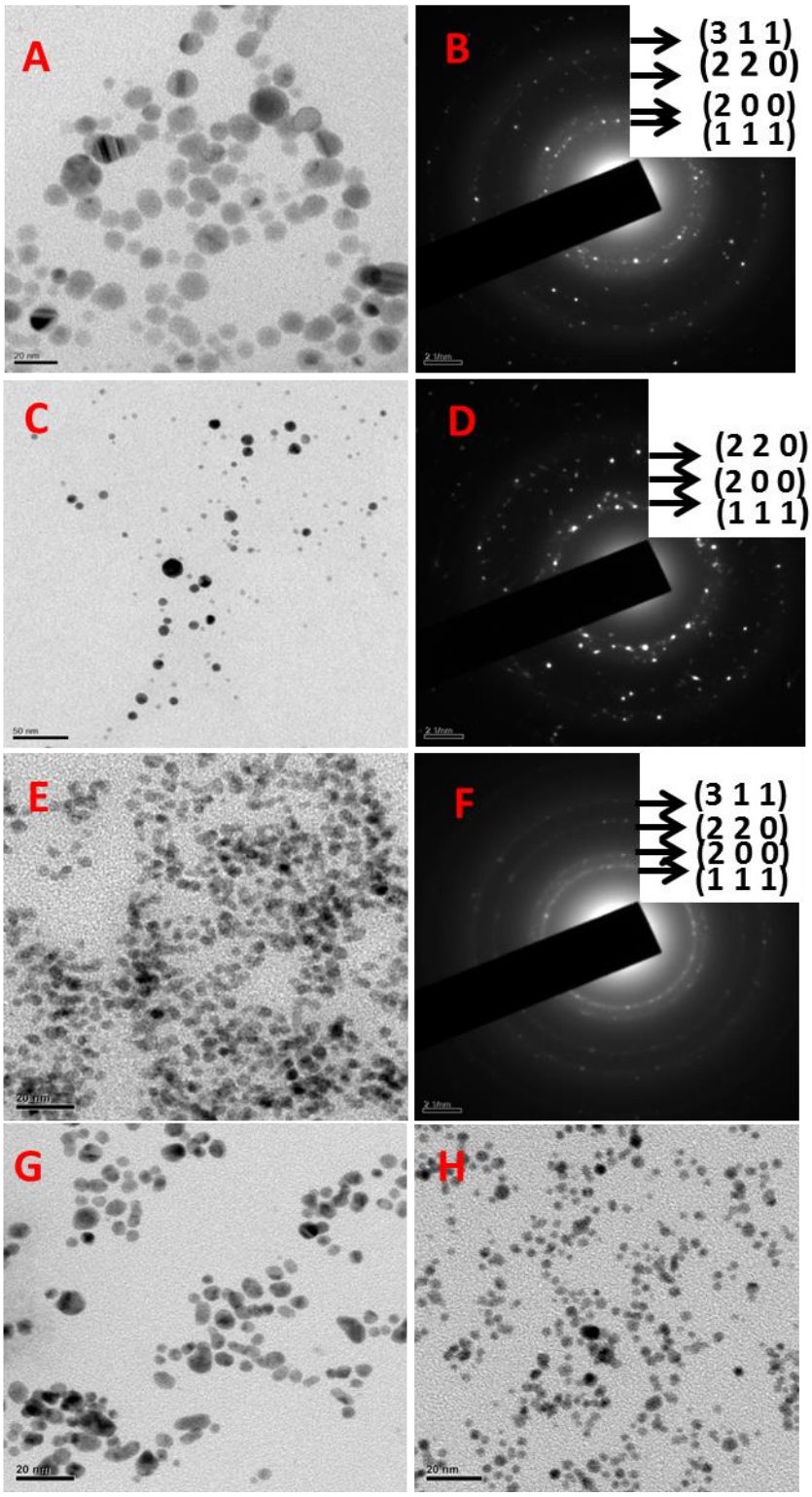

Fig. 2 HRTEM images of PADA–Ag NPs (A), PADA–Au NPs (C), PADA–$Au_{25}Ag_{75}$ NCs (E), PADA–$Au_{50}Ag_{50}$ NCs (G), and PADA–$Au_{75}Ag_{25}$ NCs (H). SEAD patterns of PADA–Ag NPs (B), PADA–Au NPs (D) and PADA–$Au_{25}Ag_{75}$ NCs (F).

3. 3 Electrochemical characterization

In order to understand the electrochemical characteristics of mono- and bi-metallic Au/Ag NCs embedded in PADA matrix, cyclic voltammograms were recorded for mono- and bi-metallic Au/Ag NCs modified GC electrodes in 0.1 M PBS. The characteristic oxidation and reduction peaks due to Au NPs present at the modified electrode were clearly observed at 0.950 and 0.414 V, respectively (Fig. 3(b)). Similarly, the characteristic oxidation peak was observed for Ag NPs at 0.252 V (Fig. 3(a)). In the case of GC/PADA–$Au_{25}Ag_{75}$ NCs modified electrode, the characteristic oxidation peak and the corresponding reduction peak were observed at 0.256 V and 0.077 V, respectively for Ag and also the oxidation and the corresponding reduction peaks for Au were observed at 0.873 V and 0.392 V, respectively along with the increment in the anodic and cathodic peak currents (Fig. 3(c)). The cyclic voltammograms recorded for the three different bi-metallic Au/Ag NCs modified electrodes are shown in Fig. S4. The characteristic oxidation and reduction peaks obtained for Au and Ag at the GC/PADA–$Au_{25}Ag_{75}$, GC/PADA–$Au_{50}Ag_{50}$ and GC/PADA–$Au_{75}Ag_{25}$ modified electrodes confirmed the presence of Au and Ag in the bi-metallic NCs. The two distinguished redox peaks and the enhanced peak currents observed for bimetallic Au/Ag NCs suggest that the NCs are in good electrical contact with the electrode.[25] Furthermore, the two distinguished redox peaks characteristics of metals were usually absent for the alloy nanostructures[26,27] and the HRTEM studies confirmed that the bi-metallic Au/Ag NCs are not the core-shell structure. Therefore, it is understand that the synthesized bi-metallic Au/Ag NCs may be hybrid nanostructures consisting both Au and Ag clusters fused together in a single particle (for a perfect alloy, it is supposed to be atom level fusion). The higher peak

currents were attributed to the catalytically active hetero-junctions between Au and Ag nanoclusters and not as mono-metal entity. Moreover, the Au-Ag bi-metallic nanostructures modified electrode may enhance the redox peak currents due to the synergistic effect of Au/Ag.

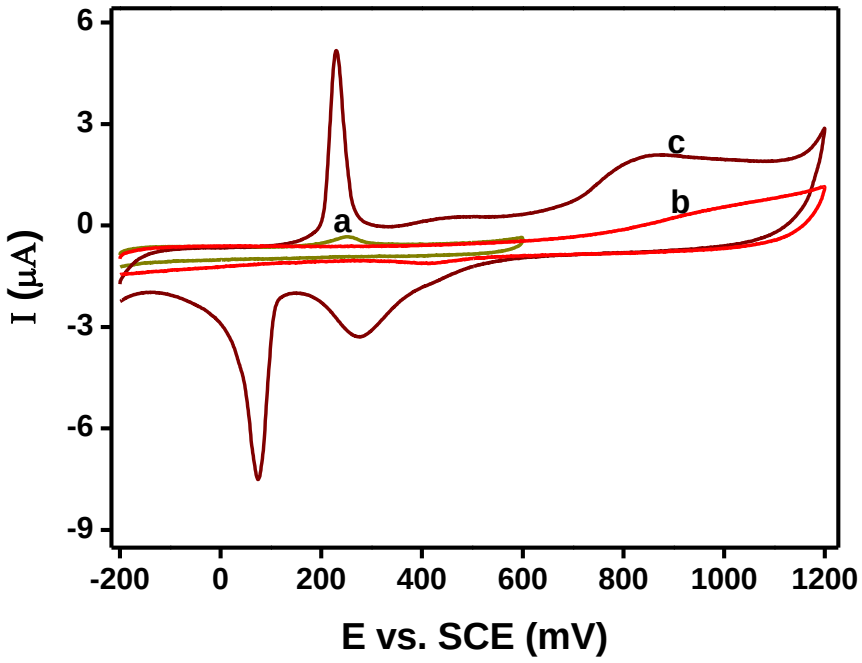

Fig. 3 Cyclic voltammograms recorded for GC/PADA–Ag NPs (a), GC/PADA–Au NPs (b) and GC/PADA–$Au_{25}Ag_{75}$ NCs (c) modified electrodes in 0.1 M PBS at a scan rate of 50 mV/s.

3. 4 Electrocatalytic oxidation of NO

The electrocatalytic oxidation of NO was carried out at the mono- and bi-metallic Au/Ag NCs modified electrodes in 0.1 M PBS (pH 7.2). Fig. 4 shows the comparison of cyclic voltammograms recorded for 100 µM NO at the GC/PADA–Ag NPs (a), GC/PADA–$Au_{25}Ag_{75}$ NCs (b), GC/PADA–$Au_{50}Ag_{50}$ NCs (c), GC/PADA–$Au_{75}Ag_{25}$ NCs (d), GC/PADA–Au NPs (e), GC/PADA (f) and bare GC (g) electrodes. As shown in Fig. 4,

electrocatalytic oxidation of NO at all the modified electrodes *via* the following reactions were observed: NO - e^- → NO^+, $NO^+ + OH^-$ → HNO_2 and HNO_2 → $H^+ + NO_2^-$.[16] In the absence of NO, no oxidation peak was observed at the GC/PADA–$Au_{25}Ag_{75}$ NCs (Fig. 4(h)) modified electrode and in the presence of NO, an observable oxidation peak was observed at 0.90 V. When compared to the GC/PADA–$Au_{25}Ag_{75}$ NCs (Fig. 4(b)) electrode, the GC/PADA–Au NPs (Fig. 4(e)) electrode showed less intense oxidation peak current for NO at 0.95 V, whereas the GC/PADA–Ag NPs (Fig. 4(a)) electrode showed almost equal current intensity but the oxidation peak potential for NO was noticed at 1.01 V. The bare GC (Fig. 4(g)) electrode and GC/PADA (Fig. 4(f)) electrode showed NO oxidation at 1.01 and 0.95 V, respectively. The observed trend from Fig. 4 clearly explains the synergistic electrocatalytic effect of the bi-metallic $Au_{25}Ag_{75}$ NCs towards NO oxidation, when compared to the mono-metallic Au and Ag NPs. Hence, the observed synergistic catalytic effect of the GC/PADA–$Au_{25}Ag_{75}$ NCs modified electrode can be attributed to the suitable composition of Au and Ag, which is responsible for the observed higher catalytic current and reduced over potential towards the NO oxidation. Among the three different Au/Ag compositions, the $Au_{25}Ag_{75}$ NCs modified electrode exhibited better catalytic response towards NO. Furthermore, the GC/PADA electrode showed better catalytic response towards NO oxidation than the bare GC electrode, which reveals the electrocatalytic and/or pre-concentrating ability of the PADA matrix. The synergistic catalytic effect of $Au_{25}Ag_{75}$ NCs was further supported by the PADA matrix at the GC/PADA–$Au_{25}Ag_{75}$ NCs electrode towards NO oxidation.

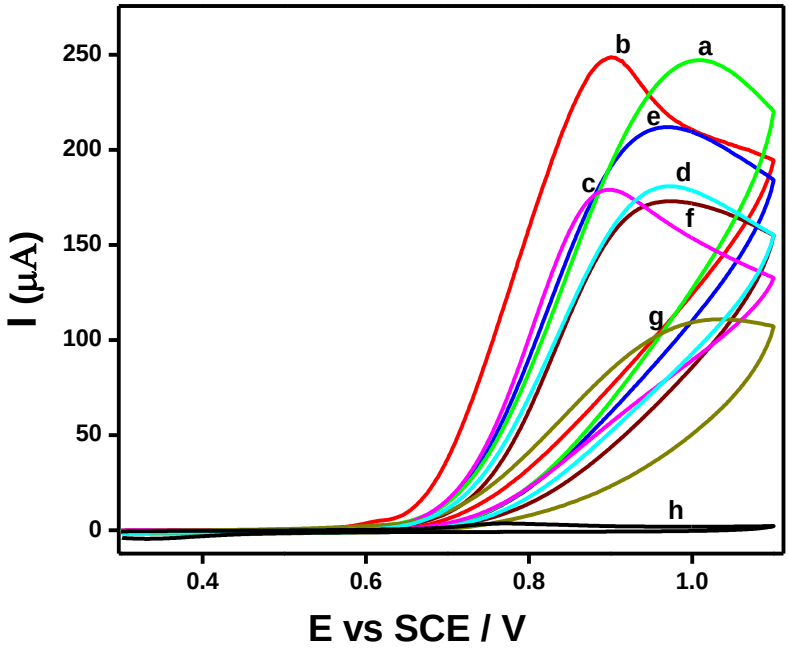

Fig. 4 Cyclic voltammograms obtained for 100 µM NO at GC/PADA–Ag NPs (a), GC/PADA–$Au_{25}Ag_{75}$ NCs (b), GC/PADA–$Au_{50}Ag_{50}$ NCs (c), GC/PADA–$Au_{75}Ag_{25}$ NCs (d), GC/PADA–Au NPs (e), GC/PADA (f) and bare GC (g) electrodes in 0.1 M PBS at a scan rate of 50 mV/s. CV obtained in the absence of NO at GC/PADA–Au_{25}/Ag_{75} NCs (h) electrode in PBS.

3. 5 Amperometric sensing of NO and interference studies

The GC/PADA–$Au_{25}Ag_{75}$ NCs modified electrode was used to prepare the amperometric sensor for the detection of NO. The amperometric *i*–*t* curve was recorded at the GC/PADA–$Au_{25}Ag_{75}$ NCs modified electrode at an applied potential of 0.9 V upon each addition of 10 nM NO to the stirred solution of 0.1 M PBS (pH 7.2) (Fig. 5(A)). The amperometric responses observed at the GC/PADA–Ag and GC/PADA–Au NPs modified electrodes are shown in Fig. S(5). Comparison of the corresponding calibration plots (concentration of NO versus current) obtained for the GC/PADA–Ag NPs, GC/PADA–Au

NPs and GC/PADA–$Au_{25}Ag_{75}$ NCs electrodes upon each addition of 10 nM NO are shown in Fig. 5(B). The GC/PADA–$Au_{25}Ag_{75}$ NCs electrode showed synergistic sensing response when compared to the mono-metallic Ag and Au NPs modified electrodes. The sensitivity of GC/PADA–$Au_{25}Ag_{75}$ NCs electrode was found to be 3.77 nA/nM (Fig. 6(B)). The amperometric *i*–*t* curve response time for 10 nM NO addition at the GC/PADA–$Au_{25}Ag_{75}$ NCs electrode is represented in the inset of Fig. 5(A) and the response time was found to be 1 s, which is much lower than the physiological lifetime (~5 s) of NO and also much lower than the reported NO detection systems (Table 1). This indicates the fast electron transfer process at the GC/PADA–$Au_{25}Ag_{75}$ NCs modified electrode.

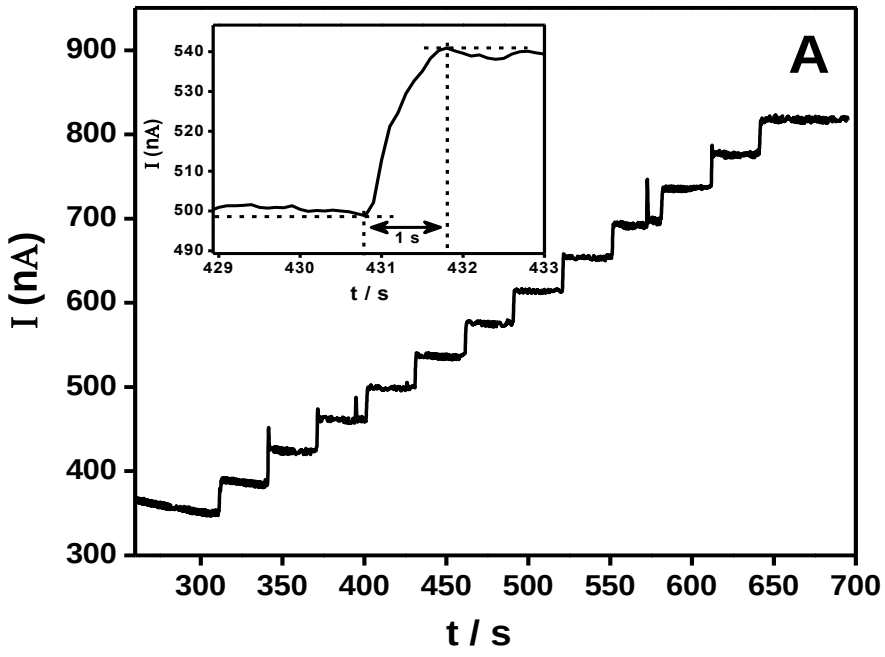

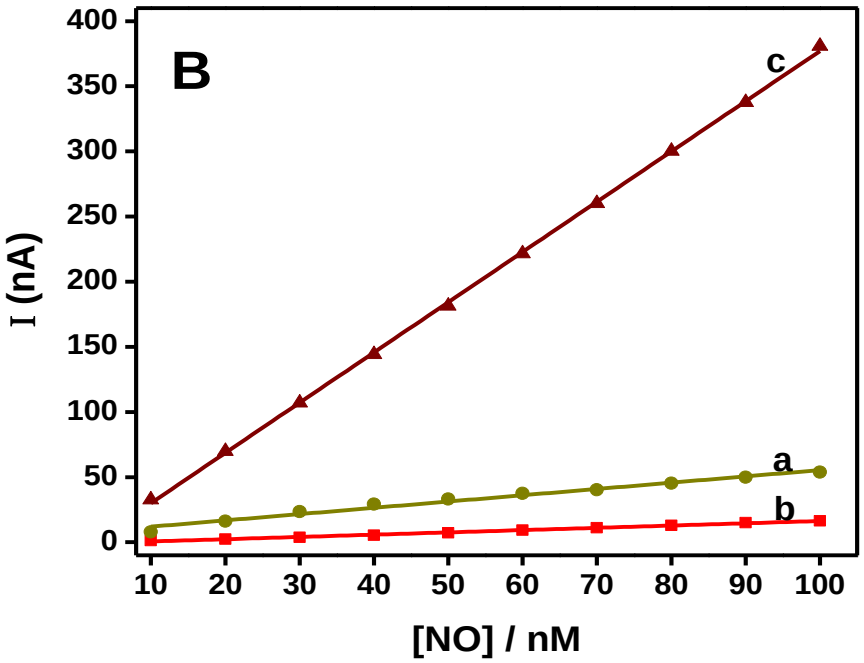

Fig. 5 (A) Amperometric *i–t* curve obtained for NO at GC/PADA–$Au_{25}Ag_{75}$ NCs electrode during the successive addition of 10 nM NO to a solution of 0.1 M PBS (pH 7.2) at an applied potential of 0.9 V. Inset: Amperometric *i–t* curve response time observed for 10 nM NO addition at the GC/PADA–$Au_{25}Ag_{75}$ NCs electrode. (B) Comparison of calibration plots of current versus NO concentration obtained for GC/PADA–Ag NPs (a), GC/PADA–Au NPs (b) and GC/PADA–$Au_{25}Ag_{75}$ NCs (c) electrodes.

Fig. 6(A) represents the amperometric *i–t* curve obtained for NO at the GC/PADA–$Au_{25}Ag_{75}$ NCs electrode during the successive addition of NO at different concentrations and the corresponding calibration plot (Fig. 6(B)) showed the linear response from 10 nM to 0.9 μM. In general, the bare electrode is often modified to eliminate interferences and to facilitate the selective detection of NO. The amperometric determination of NO in the presence of common physiological interferences such as glucose, urea, oxalate, sodium chloride, nitrate, CO_2 and NH_3 was studied at the GC/PADA–$Au_{25}Ag_{75}$ NCs electrode and the results are shown in Fig. 7. The interference study was carried out without purging N_2 gas in PBS in

order to check the interfering effect the oxygen. The addition of each 10 nM NO to the cell solution showed amperometric current response and further addition of each 100 µM of glucose (b), urea (c), oxalate (d) sodium chloride (e) and nitrate (f) followed by 1.5 µM of CO_2 (g) and 150 µM of NH_3 (h) separately at an interval of 40 s to the cell solution did not show any electrochemical response. The addition of 10 nM NO after the addition of all interferences clearly showed the amperometric current response. These observations reveal that the GC/PADA–$Au_{25}Ag_{75}$ NCs modified electrode is selective towards the determination of NO in the presence of excess physiological interferences as well as oxygen.

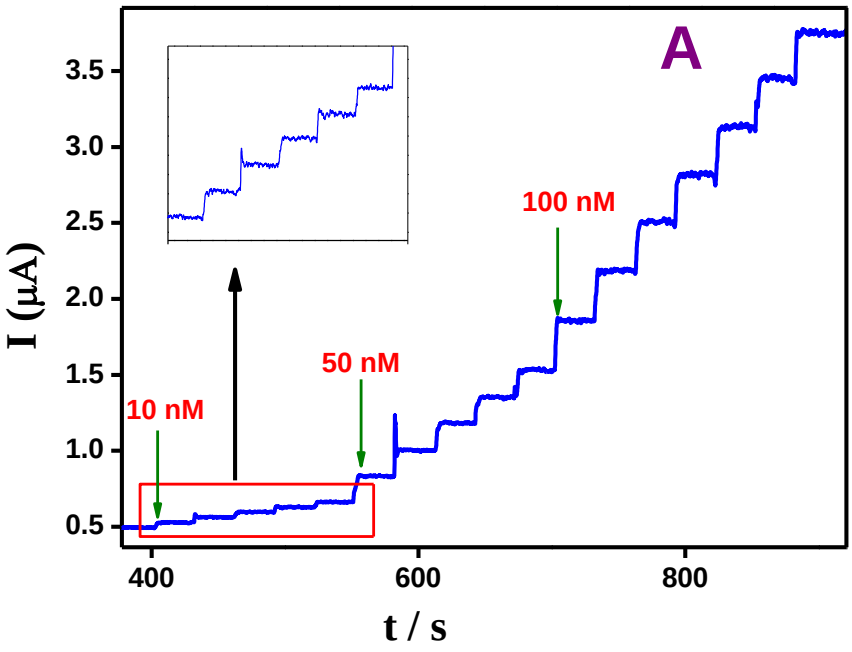

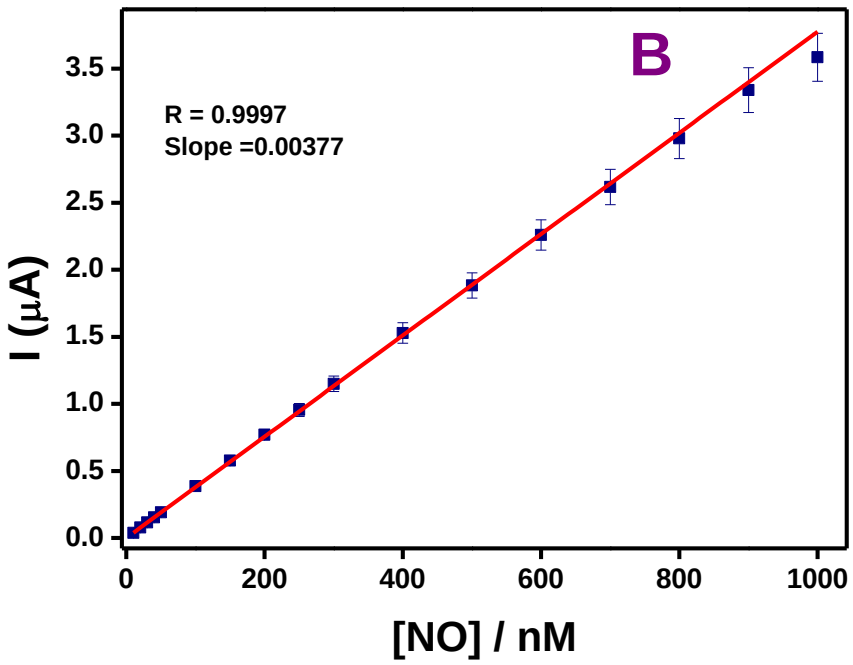

Figure 6. (**A**) Amperometric *i–t* curve obtained for NO at GC/PADA–$Au_{25}Ag_{75}$ NCs electrode during successive addition of various concentrations of NO to the solution of 0.1 M PBS (pH 7.2) at an applied potential of 0.9 V. (**B**) corresponding calibration plot.

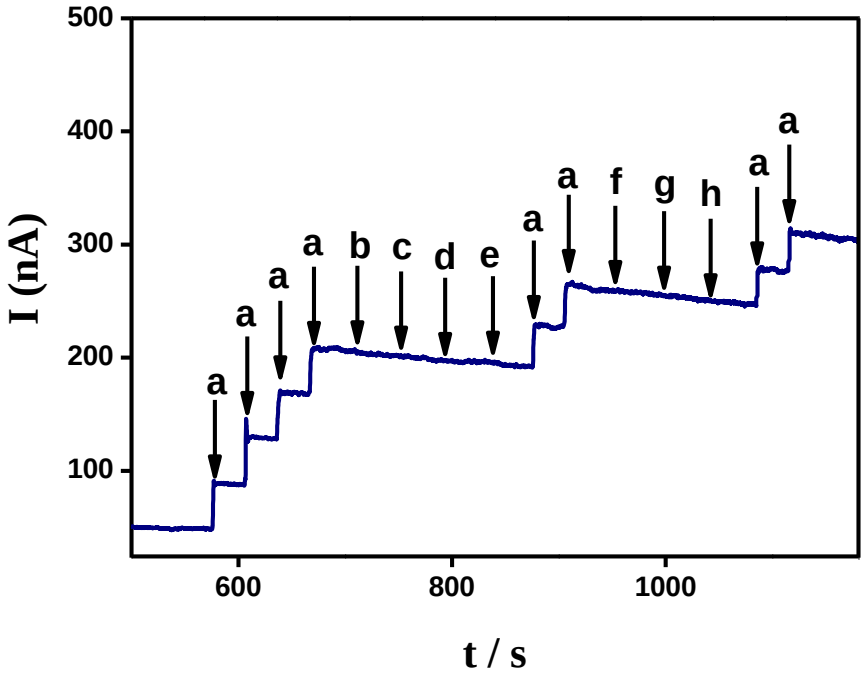

Figure 7. Amperometric *i–t* curve obtained at GC/PADA–$Au_{25}Ag_{75}$ NCs electrode in aerated solution of 0.1 M PBS (pH 7.2) at each addition of 10 nM NO (a) and each 100 µM addition of common physiological interferences such as glucose (b), urea (c), oxalate (d), sodium chloride (e) and nitrate (f) followed by 1.5 µM of CO_2 (g) and 150 µM of NH_3 (h). The applied potential was 0.9 V.

The GC electrode is the most widely used electrode for NO detection due to it is inertness, good conductivity, high hardness, high hydrogen over potential and stability. In addition, it can also be easily modified.[28] Table 1 shows the comparison of previously reported NO sensors based on metal NCs modified GCE with the present modified electrode.

Table 1. Performance comparison of NO amperometric sensors based on GC electrode modified with metal NPs.

Modified electrode	Linear range	Sensitivity	Response time (s)	S/N	[Ref]
GC/PADA–Au_{25}/Ag_{75} NCs	10nM–0.9 µM	3.77nA/nM	1	4.9	Present work

GC/RGO/Au–TPDT NRs [a]	10nM–0.14 µM	0.598nA/nM	2	–	[29]
GC/Nf–Au[b]	1nM–500 µM	–	4	3	[30]
GCE/MWNTs-Chitosan-AuNPs/Nf[c]	19 nM–54mM	1.73 µA/µM	4	3	[31]
GCE/AuNPs/MWCNT-PTTCA/MP/SOD/Catalase[d]	1.0 mM–40 mM	1.20 µA/µM	3.6	–	[32]
GCE/nano-Au	50 nM–10 mM	~0.5µA/µM	0.5 s	3	[33]
GCE/Chitosan-GNPs[e]	36.0 nM–43.2mM	0.04µA/µM	–	–	[34]

[a] RGO: Reduced graphene oxide and TPDT: tri-amine functionalized silicate sol–gel matrix. [b] Nf: Nafion membrane. [c] MWNTs: Multiwalled carbon nanotubes. [d] MP: microperoxidase, PTTCA: poly-5,2',5',2''-terthiophene-3'-carboxylic acid, SOD: Superoxide dismutase. [e] Gold nanoparticles.

4. Conclusions

The polyelectrolyte PADA matrix stabilized bi-metal Au/Ag NCs was prepared and the development of a selective and sensitive sensing platform for NO using PADA-Au/Ag NCs was demonstrated. Amperometric technique was used to sense NO and the sensitivity was found to be 3.818 nA/nM. The sensing platform was also selective and high concentration of common physiological interfering agents did not interfere with the amperometric detection of NO. The presence of a polyelectrolyte PADA matrix favored the electrocatalytic oxidation of NO at the PADA-Au/Ag NCs modified electrodes. The performance of the sensing platform was accounted by the enhancement in the S/N ratio (~4.9), fast response time (1 s) and the linear range from 10 to 4400 nM. The electrocatalytic oxidation and electrochemical sensing of NO at the bi-metallic PADA-Au/Ag NCs modified electrode showed synergistic electrocatalytic activity, sensitivity and selectivity towards NO when compared to the corresponding mono-metallic Au and Ag NPs modified electrodes.

Acknowledgments

RR acknowledges the financial support received from the Science and Engineering Research Board (SERB), New Delhi. PV is the recipient of Junior Research Fellowship under UGC-BSR scheme.

References

[1] F. H. Epstein, S. Moncada, A. Higgs, *N. Engl. J. Med.*, 1993**, 329**, 2002−2012.

[2] S. H. Snyder, *Cur. Opin. Neurobiol.*, 1992**, 2**, 3[23]−327.

[3] V. Calabrese, C. Mancuso, M. Calvani, E. Rizzarelli, D. A.Butterfield, A. M. G. Stella, *Neurotoxicity. Nat. Rev. Neurosci.*, 2007**, 8**, 766–775.

[4] K. Alving, E. Weitzberg, J. M. Lundberg, *Eur. Respir. J.*, 1993, **6**, *1368*−1370.

[5] M. Jorissen, L. Lefevere, T. Willems, *Allergy*, 2001, **56**, 1026−1033.

[6] A. W. Carpenter, M. H. Schoenfisch, *Chem. Soc. Rev.*, 2012, **41**, 3742–3752.

[7] E. M. Hetrick, M. H. Schoenfisch, *Annu. Rev. Anal.Chem.*, 2009, **2**, 409−433.

[8] Y. Lee, J. Kim, *Anal. Chem.*, 2007, **79,** 7669-7675.

[9] X. Dang, H. Hu, S. Wang, S. Hu, *Microchim. Acta*, 2015, **182,** 455–467.

[10] P. K. Rastogi, V. Ganesan and S. Krishnamoorthi, *J. Mater. Chem. A*, 2014, **2**, 933–943

[11] T. Shibata, B. A. Bunker, Z. Zhang, D. Meisel, C. F. Vardeman, J. D. Gezelter, *J. Am. Chem. Soc.*, 2002**, 124,** 11989–11996.

[12] S. Manivannan, R. Ramaraj, *J. Chem. Sci.*, 2009**, 121,** 735–743.

[13] L. Wang, F. Wang, L. Shang, C. Zhu, W. Ren, S. Dong, *Talanta*, 2010, **82**, 113–117.

[14] S. Jayabal, R. Ramaraj, *Appl. Catal., A*, 2014, **470**, 369–375.

[15] S. Jayabal, R. Ramaraj, *Electrochim. Acta*, 2013, **88**, 51–58.

[16] S. L. Tinga, C. X. Guob, K. C. Leongc, D-H. Kima, C. M. Lia, P. Chena, *Electrochim.Acta*, 2013, **111**, 441–446.

[17] L. M. Liz-Marzan, *Mater. Today*, 2004, **7**, 26–31.

[18] E. Hao, G. C. Schatz, J. T. Hupp, *J. Fluoresc.*, 2004**, 14**, 331–341.

[19] X. Liu, R. Huang, J. Zhu, *Chem. Mater*., 2008, **20,** 192–197.

[20] K, Jia, M. Y. Khaywah, Y. Li, J. L. Bijeon, P. M. Adam, R. Déturche, B. Guelorget, M. François, G. Louarn, R. E. Ionescu, ACS *Appl. Mater. Interfaces*, 2014, **6,** 219−227.

[21] S. Link, Z. L. Wang, M. A. El-Sayed, *J. Phys. Chem. B*, 1999, **103**, 3529-3533.

[22] J. J. Mock, D. R. Smith, S. Schultz, *Nano Lett.*, 2003, **3**, 1087–1090.

[23] A. Akelah, P. Kelly, S. qutubuddin, A. Moet, *Clay Miner,*. 1994, **29**, 169-178.

[24] W. P. McKenna, G. Apai, *J. Phys. Chem.*, 1992, **96**, 5902-5907.

[25] G. Maduraiveeran, R. Ramaraj, *J. Electroanal. Chem.*, 2007, **608**, 52–58.

[26] L-ur-Rahman, A. Shah, S. Bahadar Khan, A. M. Asiri, H. Hussain, C. Han, R. Qureshi, M. N. Ashiq, M. A. Zia, M. Ishaq, H-B Kraatz, *J. Appl. Electrochem.*, 2015, **5,** 463-472.

[27] S. N. Mailu, T. Waryo, P. M. Ndangili, F. R. Ngece, A. A. Baleg, P. G. Baker, E. I. Iwuoha, *Sensors*, 2010, **10**, 9449-9465.

[28] T. Xu, N. Scafa, L-P. Xu, L. Su, C. Li, S. Zhou, Y. Liu, X. Zhan, *Electroanalysis*, 2014, **26**, 449–468.

[29] S. Jayabal, P. Viswanathan, R. Ramaraj, *RSC Adv.*, 2014, **4**, 33541-33548.

[30] S. Thangavel, R. Ramaraj, *J. Phys. Chem. C*, 2008, **112**, 19825–19830.

[31] X. Deng, F. Wang, Z. Chen, *Talanta*, 2010, **82**, 1218-1224.

[32] A. A. Abdelwahab, W. C. Koh, H. B. Noh, Y. B. Shim, *Biosens. Bioelectron.*, 2010, **26**, 1080-1086.

[33] Y-J. Li, C. Liu, M-H. Yang, Y. He, E. S. Yeung, *J. Electroanal.Chem.*, 2008, **622**, 103-108.

[34] W. Fang, D. Xiaocui, W. Wei, C. Zilin, *J. Solid State Electrochem.*, 2011, **15**, 829-836.